Food Bioscience 84 (2026) 109983

Contents lists available at ScienceDirect

Food Bioscience

journal homepage: www.elsevier.com/locate/fbio

# PROSS-assisted engineering enhances the thermal and storage stability of an $AFB_1$-degrading superoxide dismutase

Yan Zhang [a], Yiqian Zhang [a], Fred Mwabulili [b], Yuhui Yang [a], Yanli Xie [a,*], Antonio Francesco Logrieco [c,**]

[a] College of Food Science and Engineering, Henan Key Laboratory of Cereal and Oil Food Safety and Nutrition, Henan University of Technology, Zhengzhou, 450001, PR China
[b] Department of Food Science and Technology, College of Agricultural Sciences and Technology, Mbeya University of Science and Technology, P.O. Box 131, Mbeya, 53119, Tanzania
[c] Xianghu Lab, Biomanufacturing Institue, Hangzhou, 311215, PR China

ARTICLE INFO

*Keywords:*
Aflatoxin $B_1$
Superoxide dismutase
PROSS
Thermostability
Storage stability

ABSTRACT

Aflatoxin $B_1$ ($AFB_1$) contamination threatens feed safety, highlighting the need for enzymatic detoxification strategies. In this study, an $AFB_1$-degrading strain, HNGD-122, was isolated and identified as a *Priestia megaterium*-related strain. Genome-guided mining identified a superoxide dismutase (SOD) with $AFB_1$-degrading activity. To improve enzyme stability, PROSS-assisted design was applied, yielding the M163K mutant. M163K retained $AFB_1$-degrading activity and exhibited enhanced thermostability, with half-lives at 70 and 80 °C extended to 32.2 and 20.7 h, respectively. It exhibited higher $AFB_1$ degradation rates than wild-type (WT)-SOD during storage at 4 °C and following freeze-drying. Molecular dynamics simulations suggested that M163K maintained SOD–$AFB_1$ interactions while improving thermostability through enhanced local stabilizing interactions. In zebrafish assays, it reduced developmental toxicity and oxidative stress after M163K treatment. In naturally contaminated corn flour and corn bran, M163K degraded approximately 66.5% and 61.9% of $AFB_1$, respectively, supporting its potential for $AFB_1$ control in corn-based feed ingredients.

## 1. Introduction

Mycotoxin contamination of staple agricultural commodities remains a major global challenge, among which aflatoxin $B_1$ ($AFB_1$) is of particular concern (Eskola et al., 2020). $AFB_1$, mainly produced by *Aspergillus flavus* and *Aspergillus parasiticus*, is one of the most hazardous and widespread mycotoxins in agricultural commodities. Owing to its well-established carcinogenic risk to humans, $AFB_1$ is listed by the International Agency for Research on Cancer (IARC) as a Group 1 carcinogen (Arsenide et al., 2006). Its toxic effects are multifaceted, including potent hepatocarcinogenicity, mutagenicity, teratogenicity, and immunosuppression. Chronic exposure to low levels of $AFB_1$ elevates hepatocellular carcinoma risk, especially in populations with prevalent hepatitis B virus infection (Benkerroum, 2020; Rushing & Selim, 2019). $AFB_1$ contamination also causes substantial economic losses by reducing the quality and marketability of maize, peanuts, cottonseed, and related commodities, leading to pre- and post-harvest losses, trade restrictions, and decreased livestock productivity. Moreover, $AFB_1$ and its metabolite aflatoxin $M_1$ ($AFM_1$) can enter animal-derived foods such as milk, thereby increasing public health risks through the food chain (Iqbal et al., 2015; Min et al., 2021). Climate change models further predict an expansion of regions suitable for aflatoxin-producing fungi, which may aggravate this problem in the future (Battilani et al., 2016; Moretti et al., 2019). Therefore, developing effective strategies to mitigate $AFB_1$ contamination is essential for global food and feed safety.

Biological detoxification of mycotoxins offers mild, selective, and eco-friendly advantages over conventional physical or chemical methods (Guan et al., 2021; Sun et al., 2023). In particular, enzymatic detoxification can transform $AFB_1$ under relatively mild conditions, thereby reducing toxin levels while minimizing adverse effects on food and feed quality. A variety of oxidoreductases have been demonstrated

* Corresponding author. College of Food Science and Engineering, Henan University of Technology, No. 100 Lianhua Street, High-tech Industrial Development Zone, Zhengzhou, 450001, Henan Province, PR China.
** Corresponding author.
*E-mail addresses:* ylxie@haut.edu.cn (Y. Xie), antoniofrancesco.logrieco@cnr.it (A.F. Logrieco).

https://doi.org/10.1016/j.fbio.2026.109983
Received 12 July 2026; Received in revised form 3 September 2026; Accepted 9 September 2026
Available online 11 September 2026

to possess $AFB_1$-degrading activity, among which laccases are one of the most extensively studied enzyme classes. For example, a laccase derived from *Bacillus amyloliquefaciens* B10 was able to effectively degrade $AFB_1$ (Xiong et al., 2022), while BsCotA from *Bacillus subtilis* exhibited high $AFB_1$-degrading efficiency in the presence of redox mediators such as methyl syringate (Wang et al., 2019). These studies have demonstrated the potential of laccases for mycotoxin biodegradation. However, the catalytic performance of different laccase systems is influenced by enzyme source, reaction conditions, and auxiliary factors, and some systems require redox mediators to achieve high degradation efficiency. Therefore, developing enzyme resources with distinct catalytic and stability characteristics from different types of oxidoreductases may help expand the enzymatic toolbox for $AFB_1$ biodetoxification and provide more options for diverse food and feed processing environments.

Superoxide dismutase (SOD) is a widely distributed metal-dependent antioxidant enzyme whose primary biological function is to catalyze the dismutation of superoxide anions and protect cells from oxidative stress. Beyond its classical antioxidant role, recent studies have revealed potential noncanonical functions of SOD in mycotoxin transformation. Previous studies, including our earlier work, have demonstrated that SODs from different microbial sources possess $AFB_1$-transforming activity. For example, an SOD from *Pseudomonas aeruginosa* HNGD-JZ06 exhibited $AFB_1$ transformation capability in a corn flour system (Ma et al., 2025), while AfSOD from *Alcaligenes faecalis* HNGD-HTN06 showed efficient $AFB_1$ transformation under near-neutral pH and elevated-temperature conditions (Hou et al., 2026). These studies indicate that SODs represent a potential enzyme resource for mycotoxin transformation and provide a foundation for further functional optimization. Unlike laccases and other extensively studied $AFB_1$-transforming oxidoreductases, SODs represent a distinct class of metal-dependent enzymes with conserved catalytic architectures and well-defined metal-associated active centers (Perry et al., 2010). These structural characteristics provide a suitable framework for rational protein engineering. However, despite the reported $AFB_1$-transforming activity of several SODs, systematic strategies for improving their thermal stability, storage stability, and operational robustness remain limited. Therefore, engineering $AFB_1$-transforming SODs with enhanced stability represents an important step toward expanding their application potential in food and feed detoxification. Although SOD has been demonstrated to participate in $AFB_1$ degradation, systematic stability engineering of $AFB_1$-degrading SODs remains relatively limited. Computational protein design provides an efficient strategy for improving enzyme stability. PROSS (Protein Repair One-Stop Shop) integrates multiple-sequence conservation analysis with structure-based energy calculations to identify amino acid substitutions that may enhance protein stability while minimizing adverse effects on catalytic sites and other key functional regions (Goldenzweig et al., 2016; Weinstein et al., 2021). This approach has been successfully applied to the stability engineering of various enzymes. For example, PROSS-assisted design improved the stability and catalytic performance of IsPETase (Rennison et al., 2021) and was also used to enhance the thermostability of a flavin-containing monooxygenase (Goris et al., 2023). Therefore, applying PROSS to the stability engineering of $AFB_1$-degrading SOD provides a rational technical strategy for improving its tolerance to elevated temperatures and its practical application performance.

In this study, an $AFB_1$-degrading strain, HNGD-122, was isolated from peanut-field soil and preliminarily identified as a Priestia megaterium-related strain. Genome-based analysis was used to identify an SOD candidate from HNGD-122, which was subsequently subjected to PROSS-assisted protein engineering to improve its stability and application performance, yielding the M163K variant. The engineering effects were then systematically evaluated in terms of thermostability, storage and freeze-drying tolerance, structural changes, product toxicity, and degradation performance in naturally contaminated corn matrices. This study extends previous research on $AFB_1$-degrading SODs from functional characterization to stability engineering and optimization of practical application performance, providing experimental support for the development of more stable SOD-based biocatalysts for $AFB_1$ detoxification.

## 2. Materials and methods

### 2.1. Isolation, screening, and identification of the $AFB_1$-Degrading strain HNGD-122

To isolate bacterial strains with potential $AFB_1$-degrading activity, 216 samples, including maize, peanut field soil, moldy maize, fermented foods, animal feces, and rotten fruits, were collected from Henan Province and surrounding regions in China. Briefly, 5.0 g of each sample was suspended in 45 mL of sterile saline and shaken at 37 °C and 180 rpm for 2–4 h. Subsequently, 200 μL of the suspension was spread onto basal salt agar plates containing coumarin as the sole carbon source to enrich microorganisms potentially capable of utilizing or transforming lactone-containing compounds (Muzaffar et al., 2025). After 24–48 h of incubation at 37 °C, colonies showing different morphological features were picked and purified through successive streaking. The purified strains were stored at −80 °C in glycerol stocks at a final concentration of 40% (v/v). For the primary $AFB_1$-removal assay, purified isolates were first cultivated overnight in LB medium under shaking conditions (37 °C, 180 rpm). For primary screening, 975 μL of overnight bacterial culture was mixed with 25 μL of an $AFB_1$ stock solution prepared from an $AFB_1$ standard (>98% purity; Sigma-Aldrich) in a final volume of 1 mL, giving a final $AFB_1$ concentration of 2.5 μg/mL. Non-inoculated LB medium containing the same amount of toxin was used as the abiotic control. After incubation at 37 °C with shaking for 72 h, the cultures were centrifuged at 12,000 × g for 10–15 min at 4 °C, and the clarified supernatants were subjected to HPLC-FLD analysis. All assays were carried out in triplicate. Isolates showing higher $AFB_1$ removal were retained for subsequent evaluation. The isolate that consistently showed strong $AFB_1$ removal in both intact culture and acellular supernatant assays was chosen for further study and named HNGD-122. After HNGD-122 had been selected based on its $AFB_1$-removing activity, its ability to degrade ZEN was additionally evaluated to characterize the broader mycotoxin-degrading phenotype of the strain. The ZEN assay was therefore performed as a post-screening characterization and was not used as a criterion for strain selection. Furthermore, the strain HNGD-122 was characterized by morphological and molecular analyses. Colony morphology was observed on LB agar plates. Cell morphology and Gram reaction were examined by Gram staining and light microscopy, and ultrastructural features were analyzed using scanning electron microscopy. For molecular identification of strain HNGD-122, the 16S rRNA and gyrB genes were amplified using genomic DNA as the template. The 16S rRNA gene was amplified using the universal primer pair 27F (5′-AGAGTTTGATCCTGGCTCAG-3′) and 1492R (5′-GGTTACCTTGTTACGACTT-3′), whereas the gyrB gene was amplified using the forward primer (5′-CCCAAGCTTAACTGCACTGGGAAATYGTHGAYAAYAG-3′) and the reverse primer (5′-CGGAATTCGGATCCACRTCGGCRTCBGTCATRAT-3′), according to the method described by Muzaffar et al. (Muzaffar et al., 2025), with minor modifications. The amplified products were verified by agarose gel electrophoresis and subjected to Sanger sequencing by Sangon Biotech Co., Ltd. (Shanghai, China). The resulting sequences were compared with homologous sequences available in the GenBank database using BLASTN. Phylogenetic trees based on the 16S rRNA and gyrB sequences were constructed using the maximum-likelihood method in MEGA, and the reliability of the tree topology was evaluated using 1000 bootstrap replicates.

### 2.2. HPLC-FLD quantification of $AFB_1$ and ZEN

After incubation, each reaction was quenched by adding methanol at the same volume as the reaction mixture. The samples were mixed thoroughly and filtered through 0.22 μm nylon membranes before

analysis on an Agilent 1260 Infinity II HPLC-FLD system. $AFB_1$ was analyzed using a ProShell 120-C18 column (150 mm × 4.6 mm, 4 μm). The mobile phase consisted of 0.1% formic acid in water and acetonitrile (55:45, v/v), delivered at 0.8 mL/min, and fluorescence detection was performed at excitation/emission wavelengths of 360/440 nm. ZEN was separated with water/methanol (20:80, v/v) at a flow rate of 1.0 mL/min and detected at 235/470 nm. The degradation rate was calculated according to the following equation:

$$D_r = \left(1 - \frac{C_1}{C_0}\right) \times 100\% \quad (1)$$

where *Dr* denotes the degradation rate of $AFB_1$ or ZEN, $C_0$ is the toxin concentration in the control, and $C_1$ is the concentration detected in the treated sample.

### 2.3. Whole-genome sequencing, assembly, and functional annotation

Genomic DNA from strain HNGD-122 that passed quality inspection was sent to Biomarker Technologies Co., Ltd. (Beijing, China) for genome sequencing. A paired-end library was prepared and sequenced on the Illumina NovaSeq 6000 platform to generate 150 bp reads, with coverage of at least 100×. Sequencing reads were inspected with FastQC v0.11.9; adapter sequences, poor-quality bases, and reads <50 bp were trimmed using Trimmomatic v0.39. Clean reads were assembled de novo in SPAdes v3.15.3, and QUAST v5.0.2 was used to summarize contig number, N50, genome length, and GC content. Genome annotation was conducted using PGAP and RAST. The predicted protein sequences were further annotated against the Nr, COG, GO, and KEGG databases using Diamond BLASTp to support functional interpretation and candidate enzyme screening. The genomic sequencing data of strain HNGD-122 have been deposited in the NCBI database under BioProject accession number PRJNA1512203.

### 2.4. Localization and characterization of mycotoxin-degrading activity

HNGD-122 cultures were centrifuged at 12,000 × g for 15 min at 4 °C. The supernatant was passed through a 0.22-μm membrane to obtain the cell-free fraction, while the collected cells were washed twice with PBS (pH 7.4) and resuspended as the cell suspension. Cells were then disrupted by sonication on ice to prepare the crude cell extract, followed by centrifugation under the same conditions to recover the soluble intracellular fraction. The fermentation broth and the resulting fractions were assayed for their ability to remove $AFB_1$ and ZEN. Unless otherwise stated, reactions were performed at 37 °C for 72 h. The cell-free supernatant was further treated by sterilization, proteinase K (PK), or SDS to assess the properties of the extracellular active components, with untreated supernatant serving as the control.

The effects of reaction conditions were examined at 30–80 °C, pH 4.0–9.0, and incubation times of 12–72 h. For the metal-ion assay, $Fe^{3+}$, $Ni^{2+}$, $Mn^{2+}$, $Cu^{2+}$, $Mg^{2+}$, $Zn^{2+}$, $Ca^{2+}$, and $Fe^{2+}$ were individually added to the reaction mixtures at the experimental concentration. Residual $AFB_1$ and ZEN were quantified by HPLC-FLD as described in Section 2.2, and degradation efficiencies were calculated relative to the corresponding toxin controls. All assays were conducted in triplicate.

### 2.5. Candidate SOD mining, heterologous expression, and protein purification

Genome annotation data of HNGD-122 were used to search for putative enzyme genes related to $AFB_1$ degradation by comparing predicted functions across the Nr, GO, KEGG, and COG databases. Together with previous laboratory observations, one SOD-encoding gene was prioritized for experimental validation. The SOD sequence was optimized for *E. coli* expression and commercially synthesized by Sangon Biotech Co., Ltd. (Shanghai, China). The fragment was cloned into pET-28a(+) (Sangon Biotech Co., Ltd., Shanghai, China) through the *Sac*I and *Not*I sites, yielding a recombinant plasmid encoding an N-terminal $His_6$-tagged SOD. After sequence confirmation, the construct was introduced into *E. coli* BL21(DE3) competent cells (Sangon Biotech Co., Ltd., Shanghai, China). Kanamycin-resistant transformants were cultured in LB medium at 37 °C and 180 rpm until the $OD_{600}$ reached 0.6–0.8. Afterwards, the recombinant expression was induced with 0.5 mmol/L IPTG at 16 °C for 18–24 h. Cells were collected by centrifugation at 8000 × g for 5–10 min at 4 °C, suspended in 50 mmol Tris-HCl buffer (pH 7.4), and lysed by sonication on ice. The crude lysate was centrifuged at 10,000–12,000 × g for 10 min at 4 °C and then filtered through a 0.45 μm membrane. The soluble His-tagged protein was purified using Ni-NTA affinity chromatography (Vazyme Biotech Co., Ltd.), washed with low-imidazole buffer, and eluted with 250 mmol imidazole. The eluted protein was concentrated and exchanged into 50 mmol Tris-HCl buffer (pH 7.4). Lastly, the protein purity was examined by 12% SDS-PAGE, and protein concentration was measured using the Bradford method. The molecular mass, theoretical pI, and other predicted physicochemical parameters were calculated with the ExPASy ProtParam tool.

### 2.6. PROSS-guided rational design and site-directed mutagenesis of SOD

To improve the thermostability of recombinant SOD, a PROSS (Protein Repair One-Stop Shop, http://pross.weizmann.ac.il)-assisted single-point mutation strategy was applied to identify potential stabilizing sites (Goldenzweig et al., 2016; Weinstein et al., 2021). The amino acid sequence and predicted structural model of SOD were submitted to the PROSS server for analysis. PROSS integrates multiple-sequence conservation information with structure-based energy evaluation to predict candidate mutations that may enhance protein folding stability. To minimize possible effects on enzyme function, metal-coordinating residues, conserved catalytic-related residues, and their neighboring regions were excluded from the mutation design. Based on the PROSS prediction results, sites predicted to improve thermostability and located away from key functional regions were prioritized for single-point mutagenesis.

Mutations were introduced into pET-28a(+)-SOD by PCR-based site-directed mutagenesis using the primer pairs shown in Table S1. After amplification, the parental methylated plasmid was digested with *Dpn*I (Sangon Biotech Co., Ltd.), and the resulting products were introduced into *Escherichia coli* DH5α competent cells (Sangon Biotech Co., Ltd.). Plasmids obtained from antibiotic-resistant colonies were confirmed by sequencing and then transformed into *E. coli* BL21 (DE3) for recombinant expression. The mutant enzymes were expressed, purified, and quantified using the same procedures applied to WT-SOD. Notably, the purified mutant proteins were verified by SDS-PAGE and then used for thermostability and $AFB_1$ degradation activity assays. The effects of PROSS-predicted mutations on SOD thermostability and catalytic performance were evaluated by comparing residual activity after heat treatment, thermal inactivation kinetic parameters, and $AFB_1$ degradation efficiency between WT-SOD and its mutants.

### 2.7. Activity and stability assays of WT-SOD and mutants

The $AFB_1$-degrading activities of WT-SOD and its variants were evaluated in 500 μL reaction mixtures containing 50 mmol buffer, 20 μg/mL enzyme, and 2.5 μg/mL $AFB_1$. Enzyme-free mixtures were included as negative controls. At the end of incubation, methanol was added at the same volume as the reaction mixture to stop the reaction. The samples were then vortexed, centrifuged, and passed through 0.22 μm nylon membranes. Then, the residual $AFB_1$ was quantified by HPLC-FLD. Enzymatic performance was reported as degradation percentage or normalized relative activity, and the highest value in each assay was taken as 100%.

The pH dependence of enzyme activity was examined in 50 mmol buffer systems, including citrate–sodium citrate (pH 4.0–5.0),

phosphate (pH 6.0), Tris-HCl (pH 7.0–8.0), and glycine–NaOH (pH 9.0–10.0). Reactions were carried out at 40 °C for 24 h. After the optimal pH was determined, the temperature profile was assessed at 20–80 °C for 24 h under the selected pH condition. To evaluate thermal tolerance, purified WT-SOD and mutant enzymes were incubated without substrate at 20–80 °C for 6 h. After heat exposure, the samples were cooled to room temperature (23-25 °C) and tested under the optimal reaction conditions. The activity of the untreated enzyme was normalized to 100%, and the remaining activity after heating was used to compare thermostability. Thermal inactivation kinetic parameters were calculated based on residual activity after heat treatment for different durations. The inactivation rate constant $k_d$ was obtained by linear fitting using the first-order inactivation equation $\ln A = -k_d \times t$, where A represents relative residual activity, and t represents the heat treatment time. The half-life ($t_{1/2}$) was calculated using the equation $t_{1/2} = \ln 2/k_d$.

To evaluate the storage stability of WT-SOD and M163K, both enzymes were stored at 4 °C for 6 weeks. The contribution of lyophilization to storage stability was further examined by vacuum freeze-drying WT-SOD and M163K, followed by storage at 4 °C for an identical duration. Aliquots were taken once per week and assayed for $AFB_1$-degrading activity under the optimized reaction conditions. Each assay included at least three replicates.

### 2.8. UPLC-QTOF-HRMS/MS analysis of $AFB_1$ transformation products

M163K was reacted with $AFB_1$ in a 500 μL system containing 2.5 μg/mL $AFB_1$, 20 μg/mL enzyme, and 50 mmol Tris-HCl buffer (pH 7.0) at 40 °C for 24 h. A reaction without enzyme was used as the control. After termination with an equal volume of methanol, samples were centrifuged and filtered through 0.22-μm membranes. $AFB_1$ transformation products were examined using an Agilent UPLC-QTOF high-resolution mass spectrometer equipped with an ESI source. Separation was performed on a CORTECS UPLC C18 column (100 mm × 2.1 mm, 1.6 μm) at 30 °C with 0.1% formic acid in water and methanol as the mobile phases at 0.3 mL/min. Spectra were collected in positive-ion mode over m/z 100–800. Selected precursor ions were subjected to collision-induced dissociation for MS/MS analysis. Product assignment was based on accurate mass, retention behavior, and MS/MS fragmentation patterns.

### 2.9. Zebrafish embryo toxicity evaluation of $AFB_1$ transformation products

To evaluate toxicity changes after enzymatic transformation, zebrafish embryos were used to compare M163K-treated $AFB_1$ products with untreated $AFB_1$. Wild-type AB and Tg(apo14) zebrafish were supplied by Nanjing Eze-Rinka Biotechnology Co., Ltd. (Nanjing, China), and the embryos were maintained in E3 medium at 28 °C. $AFB_1$ was dissolved in DMSO and diluted to 80 ng/mL. The product-treated group was prepared at the same $AFB_1$-equivalent concentration according to the initial toxin level. DMSO content was kept identical among treatments, and all product samples were processed by centrifugation, filtration, and dilution before exposure. Embryos at 24 hpf were assigned to four groups: blank control, DMSO control, $AFB_1$ exposure, and M163K-treated $AFB_1$ products. Each group contained three replicates with 30 embryos per replicate. Exposure was conducted at 28 °C for 72 h, with medium renewal every 24 h. Hepatic development and fluorescence signals were recorded by fluorescence microscopy, and liver fluorescence intensity was analyzed using ImageJ. Following exposure, larvae were rinsed with PBS, homogenized in chilled 0.9% saline, and centrifuged at 10,000 × g for 10 min at 4 °C. The supernatants were analyzed for ALT, AST, SOD, CAT, MDA, and GSH using commercial kits. Larvae were anesthetized with 300 mg/L MS-222 before imaging and sampling. All procedures were approved by the Animal Ethics Committee of Zhengzhou University (Approval No. ZZUIRB2022-92).

### 2.10. Molecular dynamics simulation

Molecular dynamics simulations were conducted with GROMACS to evaluate the $AFB_1$-complexed WT-SOD and M163K systems. The protein and catalytic copper ion were described using the CHARMM36 force field, whereas the $AFB_1$ topology was prepared with CGenFF. Each complex was placed in a dodecahedral simulation box with a minimum solute–boundary distance of 1.0 nm, solvated with the SPC/E water model, and neutralized by adding $Na^+$ and $Cl^-$ ions. Before production dynamics, the systems were subjected to steepest-descent energy minimization until the maximum force was lower than 1000 kJ $mol^{-1}$·$nm^{-1}$. Equilibration was then performed in two steps: 100 ps under the NVT ensemble at 300 K using the V-rescale thermostat, followed by 100 ps under the NPT ensemble at 1 bar with the Parrinello–Rahman barostat. Positional restraints were applied to heavy atoms during equilibration. The production run was carried out for 100 ns with a 2-fs time step under periodic boundary conditions. Particle mesh Ewald was used for long-range electrostatic interactions, and LINCS was applied to constrain bonds involving hydrogen atoms. After trajectory alignment, RMSD, RMSF, radius of gyration, hydrogen bonding, SASA, and protein–ligand interaction energy were calculated to compare conformational stability and SOD–$AFB_1$ binding behavior.

### 2.11. $AFB_1$ degradation in naturally contaminated feed samples

Feed samples naturally contaminated with $AFB_1$ were collected from a feed mill in Zhumadian, Henan Province, China, and used to evaluate the performance of M163K in a practical feed matrix. For each treatment, 2.0 g of sample was placed in a 50 mL centrifuge tube and mixed with 10 mL PBS (10 mmol/L, pH 7.2) containing 50 μg/mL M163K. The mixtures were shaken at 50 °C for 12 h. After enzyme treatment, $AFB_1$ was extracted with acetonitrile/water/acetic acid (80:19:1, v/v/v). The extracts were agitated for 20 min and centrifuged at 10,000 × g for 10 min. The collected supernatants were evaporated to dryness, and the residues were reconstituted in 1 mL of methanol. After filtration through 0.22 μm organic membranes, the samples were analyzed by HPLC-FLD. Each treatment was conducted in triplicate to reduce variation caused by the heterogeneity of naturally contaminated feed matrices.

### 2.12. Statistical analysis

Unless otherwise indicated, all assays were repeated at least three times using independent biological or technical replicates. Results are presented as mean ± SD. Statistical analyses were performed with SPSS Statistics 27.0 (IBM Corp., Armonk, NY, USA). Differences among groups were assessed by one-way ANOVA, followed by Duncan's multiple range test when significance was detected ($p < 0.05$). Graphs were generated using OriginPro 2022.

## 3. Results and discussion

### 3.1. Isolation, screening, and identification of strain HNGD-122

Biological approaches provide a relatively mild and sustainable option for controlling aflatoxin contamination in food and feed systems (Guan et al., 2021). Using the screening workflow outlined in Section 2.1, several candidate isolates were obtained from 216 environmental samples. Among them, HNGD-122 exhibited the highest $AFB_1$-degrading activity and was therefore selected for further investigation. Coumarin, a lactone-containing structural analogue, was used for the preliminary enrichment of potential $AFB_1$-degrading microorganisms (Ma et al., 2025). Morphological observation showed that HNGD-122 formed milky-white and opaque colonies on LB agar plates (Fig. 1A). Gram staining indicated that the strain was a Gram-positive rod-shaped bacterium (Fig. 1B), and scanning electron microscopy further revealed short, relatively uniform rod-shaped cells (Fig. 1C). Taken together, the

observed colony and cellular features suggested that HNGD-122 shared typical morphological traits with *Bacillus/Priestia*-related bacteria. To determine the phylogenetic affiliation of HNGD-122, 16S rRNA and gyrB sequence analyses were conducted. A clear band of approximately 1.5 kb was obtained for the 16S rRNA gene, and the corresponding phylogenetic tree showed that HNGD-122 clustered closely with *Priestia megaterium* (Fig. 1D). Considering the limited resolution of 16S rRNA sequences for distinguishing closely related *Bacillus* species, a gyrB-based phylogenetic tree was further constructed (Wang et al., 2007). The result showed that HNGD-122 was also grouped within the

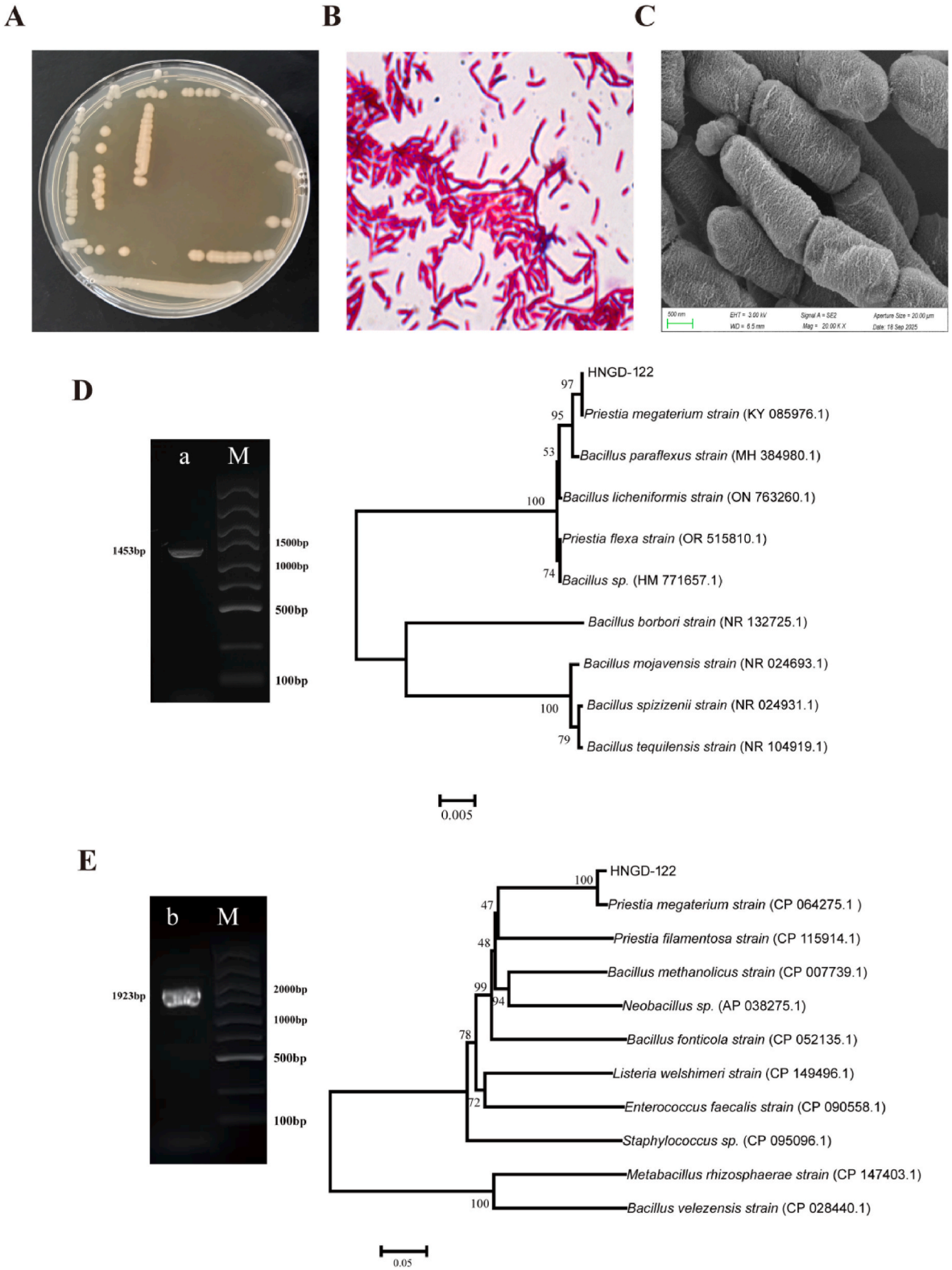


**Fig. 1.** Phenotypic observation and sequence-based identification of HNGD-122. (A) Colony appearance on LB agar plates. (B) Gram-stained cells under light microscopy. (C) Cellular morphology visualized by scanning electron microscopy. (D, E) Phylogenetic placement of HNGD-122 based on 16S rRNA and gyrB sequences, respectively.

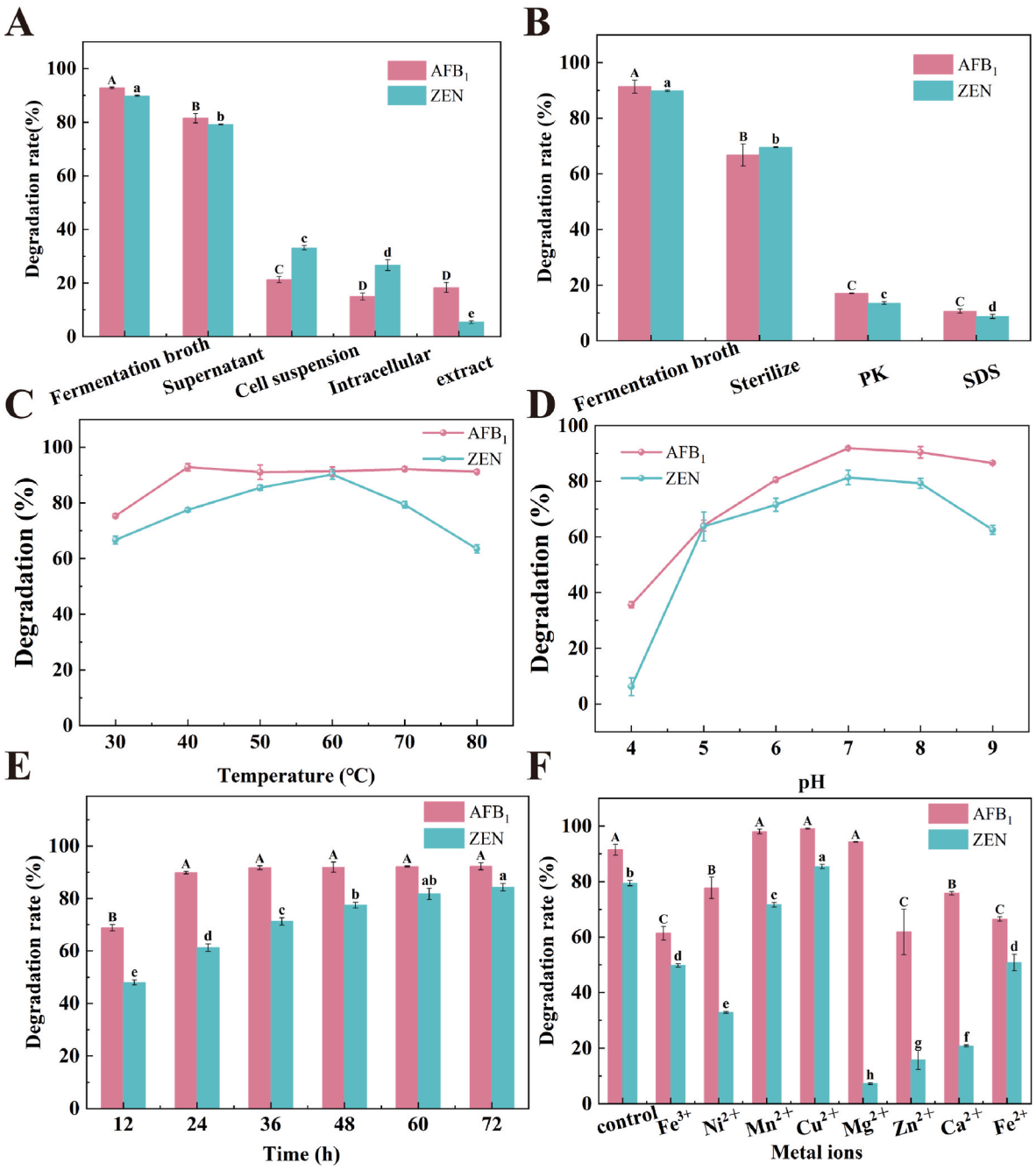


**Fig. 2.** Distribution and response profiles of $AFB_1$- and ZEN-removing activity in HNGD-122. (A) Activity distribution among fermentation broth, acellular supernatant, cell suspension, and intracellular extract. (B) Changes in activity after heat treatment, proteinase K digestion, and SDS exposure. (C–E) Effects of temperature, pH, and reaction time on $AFB_1$ and ZEN removal. (F) Modulation of degradation activity by metal ions. Uppercase letters indicate significant differences among $AFB_1$ treatment groups, whereas lowercase letters indicate significant differences among ZEN treatment groups within the same panel ($p < 0.05$). Groups sharing the same letter are not significantly different.

*P. megaterium* branch (Fig. 1E), supporting its preliminary identification as *Priestia megaterium* (formerly *Bacillus megaterium*).

Remarkably, various bacterial and fungal strains have been reported to degrade aflatoxins, among which *Bacillus*-related strains represent important candidate resources (Adebo et al., 2017). In addition, $AFB_1$-degrading enzymes have previously been mined from *Bacillus megaterium*, suggesting the potential of this bacterial group as a source of detoxification enzymes (Cheng et al., 2023). Therefore, the isolation of HNGD-122 provided a suitable enzymatic resource for subsequent genome-guided characterization and stability engineering.

### 3.2. Localization of degradation activity in HNGD-122

Microbial removal of $AFB_1$ generally involves two major processes: cellular adsorption and biotransformation, with the latter often associated with extracellular metabolites or enzymatic reactions (Verheecke et al., 2016). HNGD-122 was initially selected based on its $AFB_1$-degrading activity. In the primary screening, the strain exhibited strong $AFB_1$ degradation, reaching 92.36%. After strain selection, its degradation spectrum was further evaluated, and HNGD-122 was also found to degrade ZEN, with a degradation rate of 84.23%. Thus, the ZEN data

were included as an additional characterization of the strain-level degradation phenotype. Although HNGD-122 exhibited ZEN-removal activity at the whole-cell level, the recombinant SOD showed limited ZEN-transforming activity under the tested conditions, suggesting that other extracellular enzymes or metabolites may contribute to this phenotype. Identification of these components requires further investigation. Fig. 2A shows that strong $AFB_1$-removing activity was mainly detected in the whole fermentation broth and acellular supernatant of HNGD-122. In contrast, the cell suspension, intracellular fraction, and crude cell extract contributed only weakly to $AFB_1$ removal. These results suggest that $AFB_1$ degradation by HNGD-122 may be mainly associated with extracellular active substances. A similar distribution pattern was observed for ZEN degradation, with activity primarily detected in the fermentation broth and cell-free supernatant. Similar extracellular degradation characteristics have also been reported in *Bacillus velezensis* DY3108 and *Pseudomonas aeruginosa* M-4. (Shu et al., 2018; Xu et al., 2023).

To further characterize the extracellular active components, the cell-free supernatant was subjected to sterilization, proteinase K, and SDS treatments. As shown in Fig. 2B, sterilization reduced the degradation

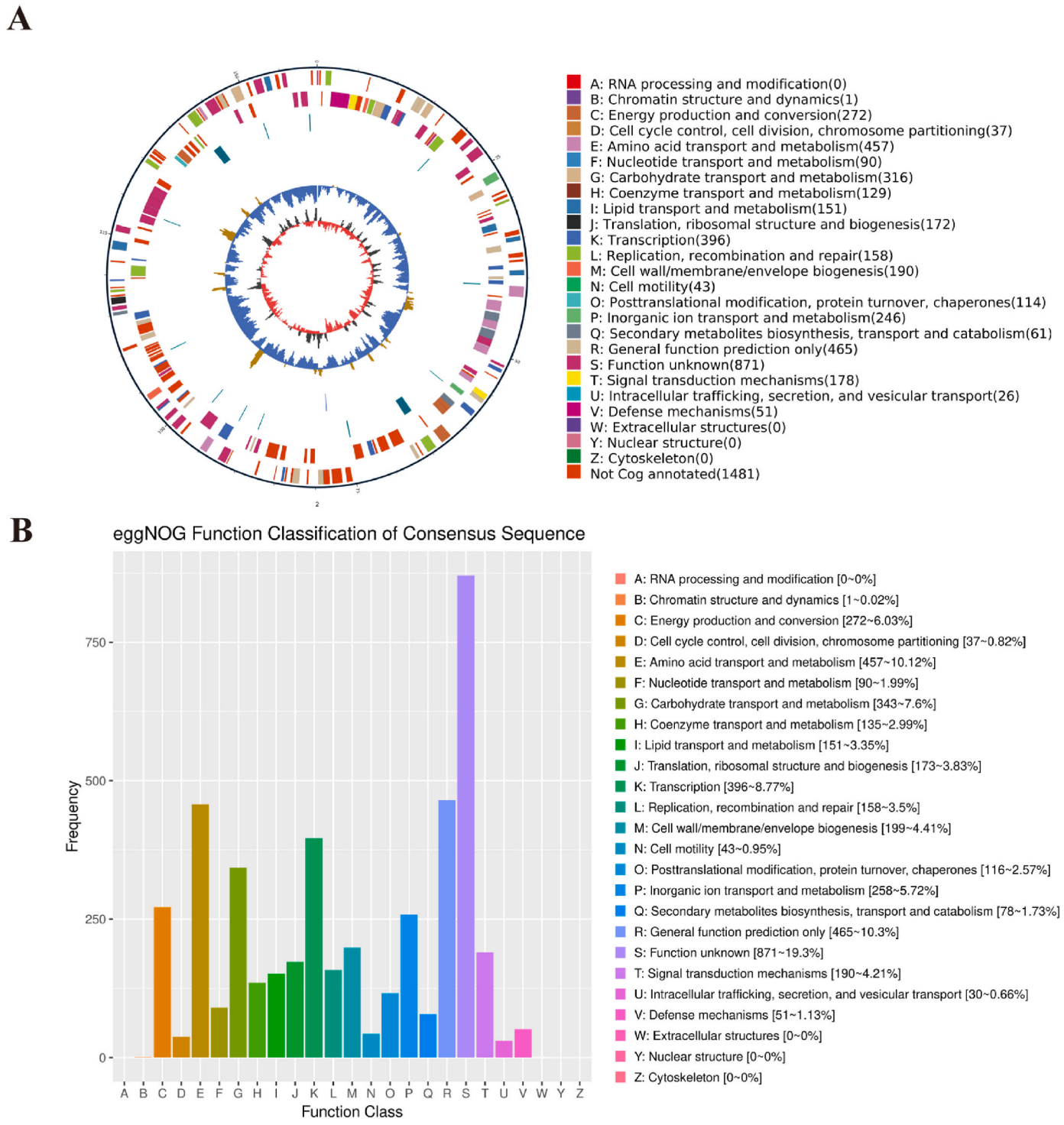


**Fig. 3.** Genome overview and functional annotation of strain HNGD-122. (A) Circular genome map of HNGD-122. (B) eggNOG-based distribution of predicted functional categories.

activities toward $AFB_1$ and ZEN but did not completely abolish them, suggesting that some active components may possess certain thermal tolerance. In contrast, proteinase K and SDS treatments markedly decreased degradation activity, indicating that proteinaceous substances played an important role in the degradation process. However, extracellular non-enzymatic metabolites have also been reported to participate in bacterial $AFB_1$ transformation; therefore, the possible involvement of non-protein components in the HNGD-122 system cannot be fully excluded (Yao et al., 2021). The reaction temperature substantially affected the degradation activity of HNGD-122. $AFB_1$ degradation remained relatively high over the range of 40–80 °C, whereas ZEN degradation reached a higher level at approximately 60 °C and then declined at higher temperatures (Fig. 2C). The pH profile showed that $AFB_1$ degradation was relatively low under acidic conditions, increased with rising pH, and remained high under neutral to weakly alkaline conditions. In contrast, ZEN degradation was most favorable around pH 7.0–8.0 (Fig. 2D). Time-course analysis showed that $AFB_1$ degradation increased rapidly during the early reaction stage and then remained at a high level from 24 h onwards, whereas ZEN degradation gradually increased with incubation time and reached a higher level at 72 h (Fig. 2E). Metal ions exerted distinct effects on degradation activity. $Cu^{2+}$, $Mg^{2+}$, and $Mn^{2+}$ generally maintained or enhanced $AFB_1$ degradation, whereas most of the tested metal ions inhibited ZEN degradation. Among them, $Cu^{2+}$ showed a comparatively less inhibitory effect on ZEN degradation (Fig. 2F). Collectively, these results indicate that $AFB_1$ degradation by HNGD-122 is mainly associated with extracellular proteinaceous active substances, providing a basis for subsequent mining of degradation enzymes.

### 3.3. Identification, recombinant expression, and purification of the candidate SOD gene

Whole-genome sequencing and functional annotation were performed for strain HNGD-122. A total of 5905 protein-coding genes were predicted in the genome of HNGD-122. The circular genome map provided an overview of the genomic organization of HNGD-122 (Fig. 3A). EggNOG annotation summarized their distribution across different functional categories (Fig. 3B), whereas GO annotation classified the predicted proteins according to biological processes, molecular functions, and cellular components (Fig. S2A). KEGG analysis further assigned the predicted proteins to major metabolic and cellular pathways (Fig. S2B). Collectively, these annotations revealed multiple genes associated with redox reactions, substance transport, and metabolic processes, providing a functional basis for subsequent candidate enzyme screening. Because genome annotation alone could not uniquely identify the enzyme responsible for $AFB_1$ degradation, candidate selection was further guided by previous functional evidence. Based on our previous findings that bacterial SODs can exhibit $AFB_1$-degrading activity, the HNGD-122 genome was specifically examined for SOD-encoding genes. A 591-bp open reading frame encoding a putative 196-amino-acid SOD was identified and selected for subsequent experimental validation. A ProtParam analysis indicated an estimated molecular mass of approximately 21 kDa and a theoretical pI of 6.19. Since this protein belongs to a metal-dependent enzyme family and may participate in redox-related reactions, it was selected for experimental verification. The gene fragment was cloned into pET-28a(+) and heterologously produced in *Escherichia coli* BL21(DE3). After IPTG induction and Ni-NTA purification, SDS-PAGE analysis revealed a clear band at approximately 21 kDa, consistent with the predicted molecular mass and confirming the successful expression and purification of recombinant SOD. (Fig. S1). Functional evaluation of the purified recombinant SOD showed clear degradation activity toward $AFB_1$, whereas no effective ZEN-degrading activity was observed under the tested conditions. These results suggest that the ZEN-degrading phenotype of HNGD-122 may involve other active components rather than the identified SOD. Accordingly, subsequent enzymatic characterization, PROSS-assisted engineering, degradation-product identification, toxicity evaluation, and practical application experiments were focused on $AFB_1$.

### 3.4. Enzymatic properties of SOD

To characterize the $AFB_1$-degrading properties of SOD derived from HNGD-122, the effects of reaction temperature, thermostability, pH, pH stability, metal ions, and incubation time on its degradation activity were systematically investigated. Factors such as temperature, pH, and metal ions can influence enzyme conformational stability, substrate binding, and catalytic efficiency, and are therefore important parameters for evaluating enzymatic performance and application potential (Lyagin & Efremenko, 2019).

Reaction temperature had a pronounced influence on SOD-mediated $AFB_1$ removal (Fig. 4A). The maximum degradation efficiency was observed at 40 °C, where approximately 92.45% of $AFB_1$ was removed. As the temperature was further raised from 50 to 80 °C, the degradation efficiency decreased progressively; however, the enzyme still retained approximately 67.74% degradation activity at 80 °C, indicating that it maintained partial catalytic capacity under elevated temperatures. Previous studies have shown that SOD-like enzymes can participate in $AFB_1$ degradation, suggesting that they may represent promising enzymatic resources for mycotoxin biodegradation (Ma et al., 2025). Thermal stability assays further demonstrated that SOD retained considerable activity after incubation without substrate at 20–70 °C for 6 h. Even after a 6 h incubation at 80 °C, the enzyme retained approximately 56.56% of its activity (Fig. 4B). These findings suggest that HNGD-122-derived SOD possesses moderate thermal tolerance, although prolonged exposure to high temperature still causes activity loss. The pH strongly influenced SOD-mediated $AFB_1$ removal (Fig. 4C). Under acidic conditions, the enzyme displayed weak activity, whereas $AFB_1$ degradation increased as the reaction environment approached neutrality. The highest activity was observed at pH 7.0, with a degradation rate of approximately 92.05%. SOD also remained highly active at pH 8.0, but more acidic or alkaline environments caused a pronounced activity loss. The pH stability assay further showed that the enzyme was better preserved within pH 6.0–8.0, with maximal residual activity after treatment at pH 7.0, while strong alkaline exposure reduced its stability (Fig. 4D). Metal ions significantly affected SOD degradation activity (Fig. 4E). Among the tested additives, $Cu^{2+}$ produced the strongest enhancement, with relative activity reaching approximately 92.89%, exceeding that of the untreated control. $Mn^{2+}$ and $Zn^{2+}$ caused only minor changes, whereas $Mg^{2+}$ and EDTA clearly suppressed SOD activity. Previous studies have shown that metal ions, mediators, and redox conditions can influence the catalytic efficiency of certain aflatoxin-degrading enzymes, which is often associated with electron transfer, redox reactions, or enzyme conformational stability (Kumar et al., 2022). Therefore, the $Cu^{2+}$ sensitivity observed in HNGD-122-derived SOD may be related to metal-assisted maintenance of catalytic conformation or redox processes, although the underlying mechanism requires further verification. Time-course analysis showed that $AFB_1$ degradation by SOD was clearly time dependent (Fig. 4F). The degradation rate was relatively low during the early stage of the reaction and gradually increased with prolonged incubation, reaching approximately 93.04% at 24 h and further increasing to 99.23% at 36 h, indicating that $AFB_1$ degradation continued beyond 24 h and approached a plateau by 36 h. Overall, HNGD-122-derived SOD exhibited optimal $AFB_1$ degradation activity at 40 °C and pH 7.0, together with moderate thermal tolerance, near-neutral pH preference, $Cu^{2+}$ sensitivity, and time-dependent degradation behavior. These enzymatic characteristics provide an experimental basis for subsequent stability engineering and application evaluation.

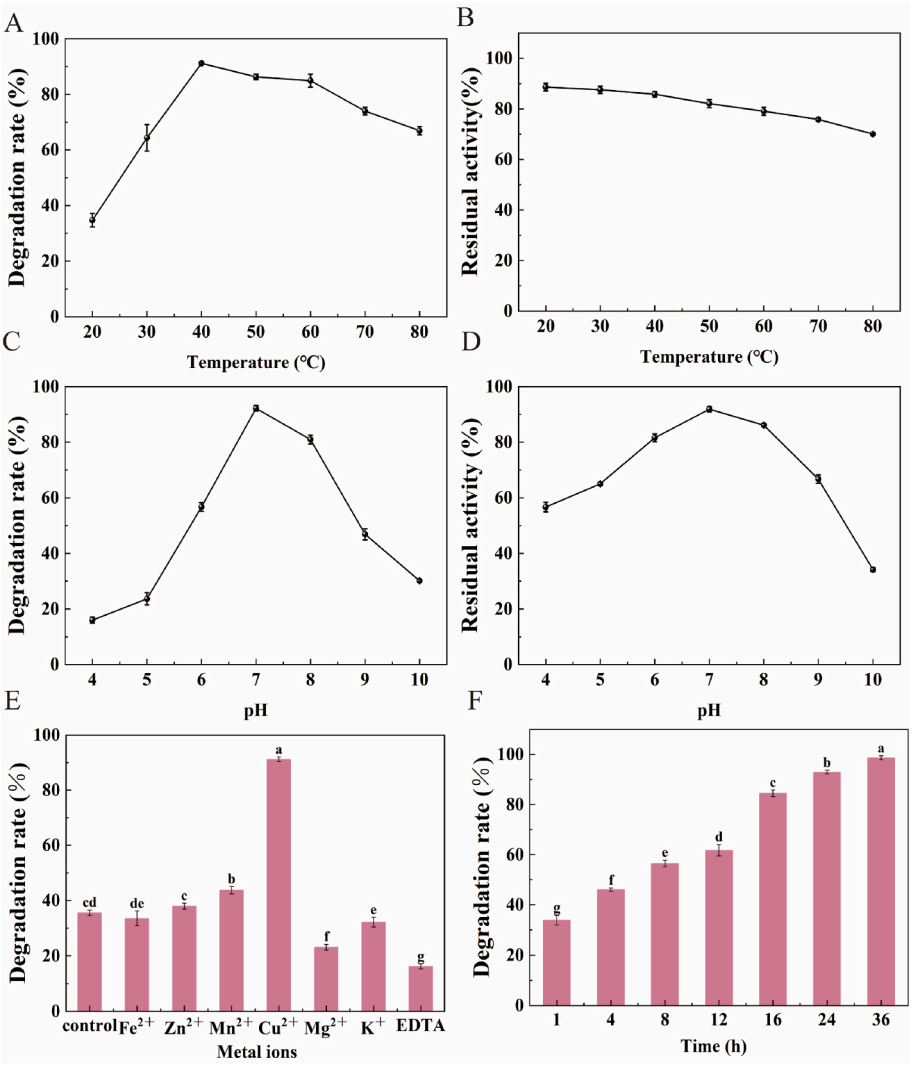


**Fig. 4.** Biochemical profile of HNGD-122-derived SOD during $AFB_1$ removal. (A) Temperature-dependent $AFB_1$ removal. (B) Remaining activity after heat exposure. (C, D) pH-dependent activity and pH tolerance. (E) Modulation of SOD activity by metal ions and EDTA. (F) Time-course pattern of $AFB_1$ degradation. Different lowercase letters within each panel indicate significant differences among the corresponding groups according to one-way ANOVA followed by Duncan's multiple range test ($p < 0.05$), whereas groups sharing the same letter are not significantly different.

### *3.5. Screening, expression, and thermostability evaluation of PROSS-designed mutants*

Based on the PROSS design results, candidate SOD single-point mutants were constructed and expressed to evaluate whether stabilizing mutations affected $AFB_1$ degrading rate. The mutations produced different effects on $AFB_1$ degradation rates (Fig. 5A). Although several variants showed comparable $AFB_1$-degrading activities in the initial screening, M163K exhibited the highest mean degradation rate and showed superior activity retention after incubation at 70 °C for 6 h in the preliminary thermal-tolerance screening (Table S2). Considering both $AFB_1$-degrading activity and thermal tolerance, M163K was therefore selected for subsequent detailed characterization. Thermal tolerance was evaluated by exposing WT-SOD and M163K to a range of temperatures for 6 h, followed by the determination of the remaining $AFB_1$-degrading activity. As shown in Fig. 5B, M163K retained higher residual activity than WT-SOD over the temperature range of 20–80 °C. At 70 and 80 °C, WT-SOD retained approximately 76.87 and 70.62% of its activity, respectively, whereas M163K retained approximately 88.09% and 82.66%, indicating that M163K exhibited stronger tolerance to heat treatment. To characterize thermal deactivation, WT-SOD and M163K were heated at 70 or 80 °C for selected time intervals, and residual activity was recorded. The rate constant $k_d$ and half-life $t_{1/2}$ were derived by fitting the data to a first-order inactivation equation. At 70 °C, WT-SOD showed a $k_d$ value of 0.0456 $h^{-1}$ and a $t_{1/2}$ of 15.2 h, whereas M163K showed a lower $k_d$ value of 0.0215 $h^{-1}$ and an extended $t_{1/2}$ of 32.2 h, representing a 2.12-fold increase compared with WT-SOD (Fig. 5C). At 80 °C, the $k_d$ value of WT-SOD was 0.0597 $h^{-1}$, with a $t_{1/2}$ of 11.6 h, whereas M163K showed a reduced $k_d$ value of 0.0335 $h^{-1}$ and an extended $t_{1/2}$ of 20.7 h, corresponding to a 1.78-fold increase (Fig. 5D). These results indicate that M163K slowed the thermal inactivation of SOD under high-temperature conditions.

The storage stability of WT-SOD and M163K was evaluated at 4 °C for 6 weeks. After 6 weeks, the $AFB_1$ degradation rates of WT-SOD and M163K decreased to 50.26% and 67.17%, respectively (Fig. 5E). For the freeze-dried enzymes, the corresponding degradation rates were 58.74% and 74.63%, respectively (Fig. 5F), indicating improved storage stability after lyophilization. These results indicate that M163K exhibited improved storage stability and that lyophilization further reduced activity loss. This improvement may be associated with enhanced

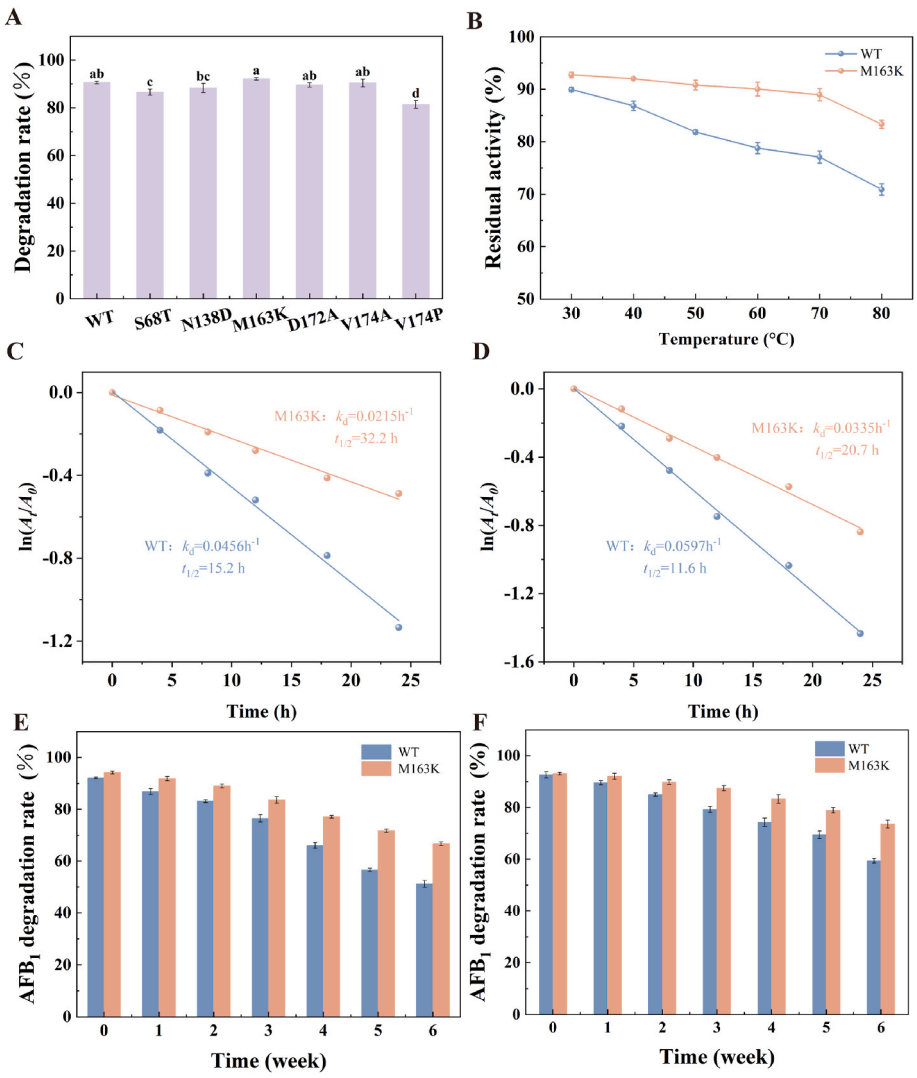


**Fig. 5.** Screening and stability evaluation of SOD mutants. (A) $AFB_1$ degradation rate of WT-SOD and selected mutants. (B) Residual $AFB_1$ degradation activities of WT-SOD and M163K after incubation at different temperatures. (C, D) First-order thermal inactivation fitting of WT-SOD and M163K at 70 °C and 80 °C, respectively. (E) $AFB_1$ degradation rates of free WT-SOD and M163K during storage at 4 °C. (F) $AFB_1$ degradation rates of freeze-dried WT-SOD and M163K during storage at 4 °C. Different letters indicate significant differences ($p < 0.05$).

conformational stability and reduced molecular mobility during storage and freeze-drying (Arsiccio et al., 2020; Bhatnagar et al., 2007; Karunnanithy et al., 2024).

Overall, M163K substantially improved the thermal and storage stability of the HNGD-122-derived SOD while largely retaining its $AFB_1$-degrading activity, as evidenced by its prolonged half-lives at 70 and 80 °C and higher $AFB_1$ degradation rates during storage at 4 °C and after freeze-drying. Previous studies have demonstrated that SODs from different microbial sources can participate in aflatoxin transformation. In the present study, an SOD with $AFB_1$-degrading activity was identified and functionally validated from the *Priestia megaterium*-related strain HNGD-122, further expanding the microbial sources of $AFB_1$-degrading SODs. More importantly, PROSS-assisted stability engineering was applied to this enzyme to improve its stability and practical performance. These findings extend previous functional studies of $AFB_1$-degrading SODs toward protein stability engineering and demonstrate that computationally guided design can improve the adaptability of these enzymes to processing, storage, and formulation conditions.

### *3.6. Identification and toxicity evaluation of $AFB_1$ degradation products*

To elucidate the transformation pattern of $AFB_1$ mediated by M163K and assess the associated toxicity changes, high-resolution LC-MS/MS analysis and a zebrafish embryo model were employed. The toxicity of $AFB_1$ is mainly associated with its difuran ring, C8=C9 double bond, coumarin lactone moiety, and cyclopentenone structure. Oxidation, hydroxylation, or ring-opening modifications of these key structural regions are generally considered closely related to toxicity attenuation. In the M163K-treated $AFB_1$ reaction system, a major transformation product was further characterized by high-resolution mass spectrometry. The product exhibited a protonated molecular ion $[M + H]^+$ at m/z 329.06543 and a sodium adduct $[M + Na]^+$ at m/z 351.04742, consistent with the molecular formula $C_{17}H_{12}O_7$ (Fig. 6). The approximately 16 Da mass increase relative to protonated $AFB_1$ was consistent with the incorporation of one oxygen atom. Subsequent MS/MS analysis of the precursor ion revealed characteristic fragment ions at m/z 311.05612 and 283.06207 (Fig. S3). The fragment ion at m/z 311.05612 was

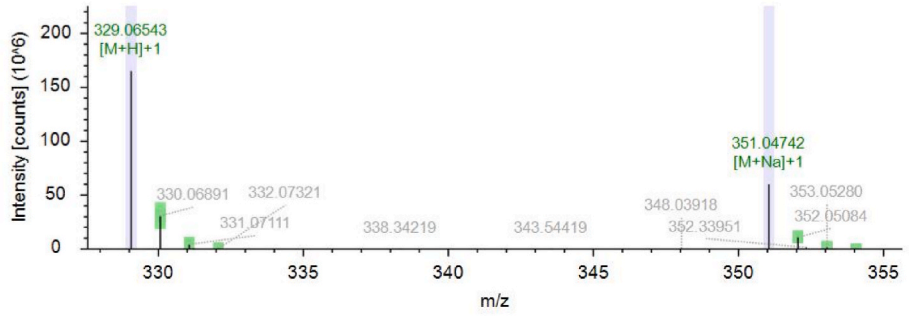


**Fig. 6.** High-resolution mass spectrum of the putative $AFQ_1$ generated during M163K-mediated $AFB_1$ degradation.

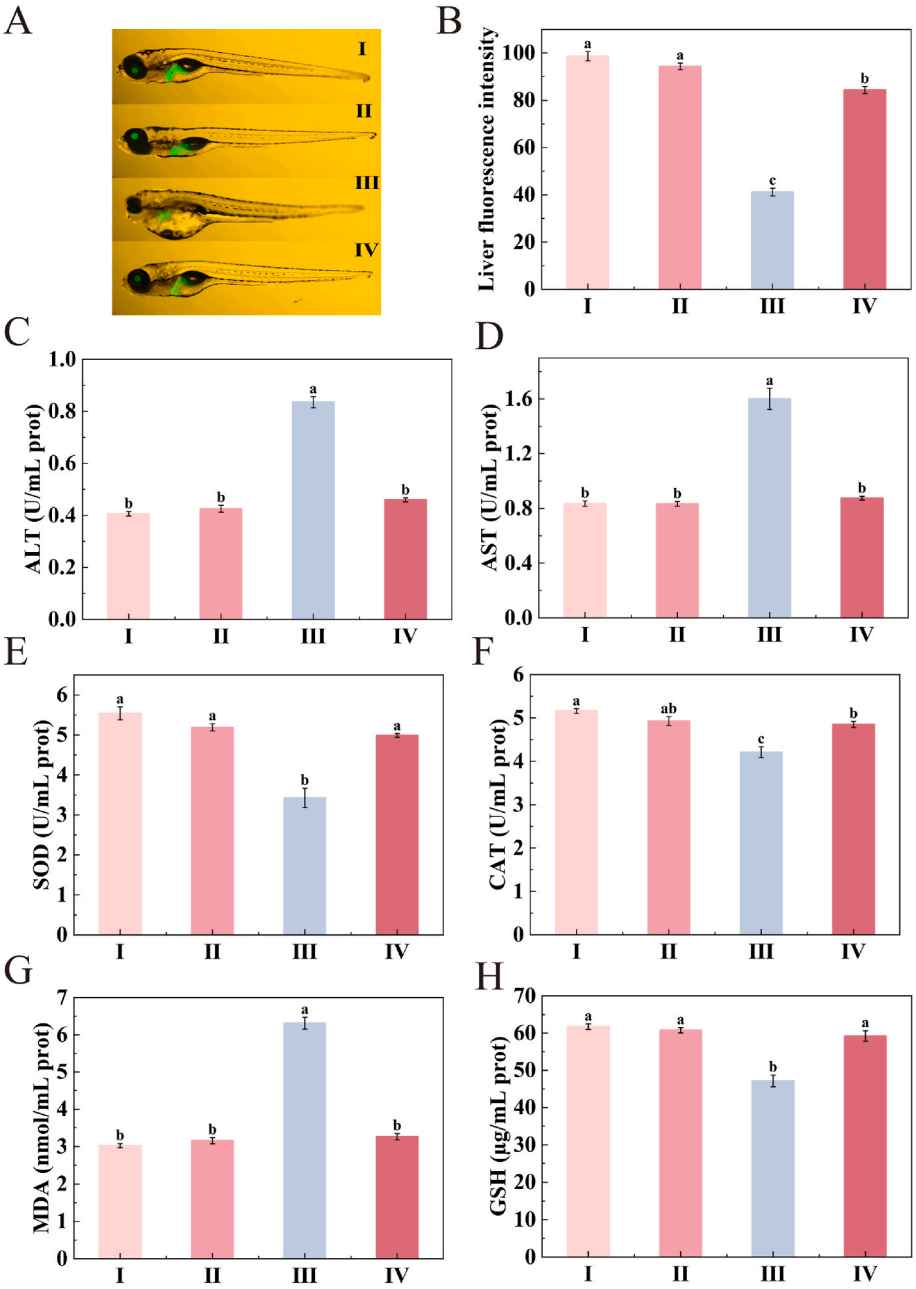


**Fig. 7.** Toxicological evaluation of $AFB_1$ transformation products in zebrafish larvae. (A) Representative images of liver-fluorescent zebrafish larvae. (B) Quantification of hepatic fluorescence intensity. (C–H) Changes in ALT, AST, SOD, CAT, MDA, and GSH levels. Groups: I, control; II, DMSO; III, $AFB_1$; IV, M163K-treated $AFB_1$ products. Different letters indicate significant differences ($p < 0.05$).

consistent with the neutral loss of $H_2O$, and the overall fragmentation pattern was consistent with previously reported MS/MS characteristics of $AFQ_1$. The putative $AFQ_1$ product exhibited a retention time of approximately 4.98 min, as shown in Fig. S4. Based on the accurate mass, molecular formula, MS/MS fragmentation pattern, and retention behavior, together with comparison with previously reported $AFB_1$ transformation products, the compound was tentatively identified as $AFQ_1$. Previous studies have reported the formation of $AFQ_1$-related products during enzymatic transformation of $AFB_1$ by laccases and multicopper oxidases (Qin et al., 2021; Zhang et al., 2026), further supporting this assignment. $AFQ_1$ is a hydroxylated derivative of $AFB_1$ and has been reported to exhibit lower toxicity than the parent $AFB_1$ (Mwabulili et al., 2026). Therefore, the formation of this hydroxylated product suggests that M163K may mediate $AFB_1$ transformation through an oxidation/hydroxylation process. Because an authentic $AFQ_1$ standard and NMR confirmation were not available in the present study, the structural assignment should be considered tentative, and definitive identification would require further confirmation using an authentic standard and/or NMR analysis.

To further evaluate the toxicity changes after M163K-mediated $AFB_1$ transformation, a zebrafish embryo model was used. As shown in Fig. 7, embryos in the CK group (I) and DMSO group (II) developed normally and showed strong hepatic fluorescence signals, indicating that the solvent treatment had limited effects on embryonic development. In contrast, the $AFB_1$ exposure group (III) showed obvious developmental abnormalities, including body axis curvature, yolk sac edema, and reduced hepatic fluorescence intensity. Biochemical measurements further revealed elevated ALT, AST, and MDA levels, accompanied by reduced SOD, CAT, and GSH levels, suggesting that $AFB_1$ exposure caused hepatic damage and oxidative imbalance. Compared with the $AFB_1$ exposure group, the degradation product group treated with M163K (IV) exhibited alleviated morphological abnormalities and partial recovery of hepatic fluorescence signals. In addition, ALT, AST, and MDA levels decreased, while SOD, CAT, and GSH levels increased. Collectively, these results indicate that the M163K-treated $AFB_1$ transformation products exhibited reduced developmental toxicity and hepatotoxicity and induced lower oxidative stress than untreated $AFB_1$ in the zebrafish embryo model. These findings suggest that M163K-mediated transformation contributes to the attenuation of $AFB_1$ toxicity.

### 3.7. Application of M163K in $AFB_1$-Contaminated corn-based feed ingredients

$AFB_1$ is a common contaminant in maize and its by-products and can affect animal health through the feed chain, thereby posing a potential risk to food safety (Mahato et al., 2019; Pożarska et al., 2024). To evaluate the $AFB_1$-degrading capacity of M163K in practical feed matrices, naturally $AFB_1$-contaminated corn flour and corn bran were selected as representative corn-based feed ingredients. As shown in Fig. 8, the initial $AFB_1$ contents in corn flour and corn bran were approximately 882.45 and 706.47 μg/kg, respectively. After treatment with M163K, the residual $AFB_1$ levels decreased to approximately 295.26 and 268.85 μg/kg, corresponding to degradation rates of approximately 66.5% and 61.9%, respectively. These results indicate that M163K retained $AFB_1$-degrading activity in naturally contaminated corn-based feed matrices. The differences in degradation efficiency between matrices may be related to sample composition, particle structure, water absorption capacity, and the binding state of $AFB_1$. Previous studies have shown that the release and accessibility of mycotoxins can be influenced by food matrices and contamination patterns (Escrivá et al., 2021). Compared with liquid reaction systems, part of the $AFB_1$ in naturally contaminated feed ingredients may be associated with starch, protein, or fiber components, thereby limiting its release into the aqueous phase and reducing enzyme–substrate contact. Similarly, Ery4 laccase was reported to completely remove $AFB_1$ in buffer, whereas its degradation efficiency was markedly reduced in contaminated maize, suggesting that practical matrices can affect enzymatic detoxification efficiency (Loi et al., 2023). In addition, engineered laccase has been applied to $AFB_1$ degradation in contaminated corn flour and corn bran, and its degradation efficiency in real maize matrices was also lower than that observed in in vitro reaction systems (Zhang et al., 2026).

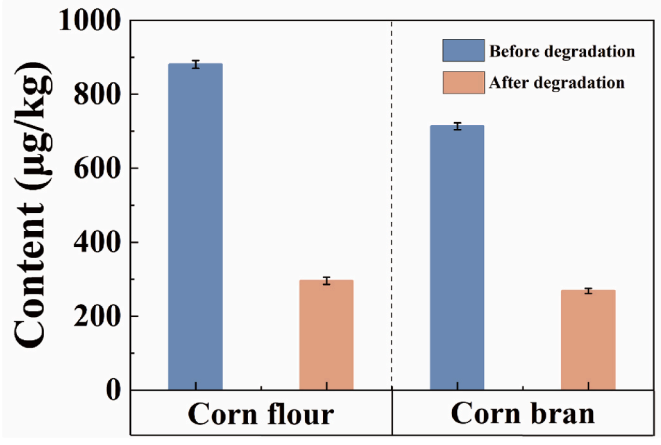


**Fig. 8.** Application of M163K in $AFB_1$-contaminated corn-based feed ingredients. $AFB_1$ contents in corn flour and corn bran before and after enzymatic treatment.

Overall, M163K effectively reduced $AFB_1$ residues in corn flour and corn bran, suggesting its potential application in the detoxification of corn-based feed ingredients. According to the Chinese national standard GB 13078-2017 (Hygienical Standard for Feeds), the maximum permitted level of $AFB_1$ in corn-processing products used as feed materials is 50 μg/kg. Although M163K substantially reduced $AFB_1$ contamination in both matrices, the residual concentrations under the current experimental conditions remained above this regulatory limit. Therefore, future studies should focus on optimizing enzyme dosage, reaction time, moisture conditions, and treatment strategies to further improve $AFB_1$ removal efficiency and reduce residual $AFB_1$ toward regulatory-compliant levels, thereby facilitating the practical application of M163K in feed detoxification.

### 3.8. MD-based structural assessment of WT-SOD and M163K

Because MD simulation provides atomistic insight into protein motion, stability, and enzyme–ligand interactions (Hollingsworth & Dror, 2018), the WT-SOD–$AFB_1$ and M163K–$AFB_1$ systems were simulated to clarify how the M163K substitution affected conformational stability and $AFB_1$ binding behavior (Fig. 9). RMSD analysis showed that both systems rapidly reached equilibrium during the simulation (Fig. 9A). Compared with WT-SOD, M163K exhibited lower fluctuation, suggesting improved overall conformational stability. RMSF analysis further showed reduced residue-level flexibility in several regions of M163K (Fig. 9B), indicating that the mutation may restrict local structural motion. In addition, M163K showed a lower and more stable radius of gyration (Fig. 9C), suggesting a more compact protein conformation. The interaction energy between SOD and $AFB_1$ showed no marked difference between the WT and M163K systems (Fig. 9D), indicating that the mutation did not substantially disturb the SOD–$AFB_1$ interaction. Hydrogen bond analysis showed that the number of hydrogen bonds in the M163K system was comparable to or slightly higher than that in WT-SOD (Fig. 9E), which may contribute to structural stabilization. The solvent-accessible surface area (SASA) of M163K was also slightly reduced (Fig. 9F), further supporting enhanced conformational compactness and reduced solvent exposure. Mechanistically, the M163K mutation replaces methionine with lysine, thereby introducing a positively charged side chain. This substitution may alter the local interaction network around the mutation site and promote the formation of

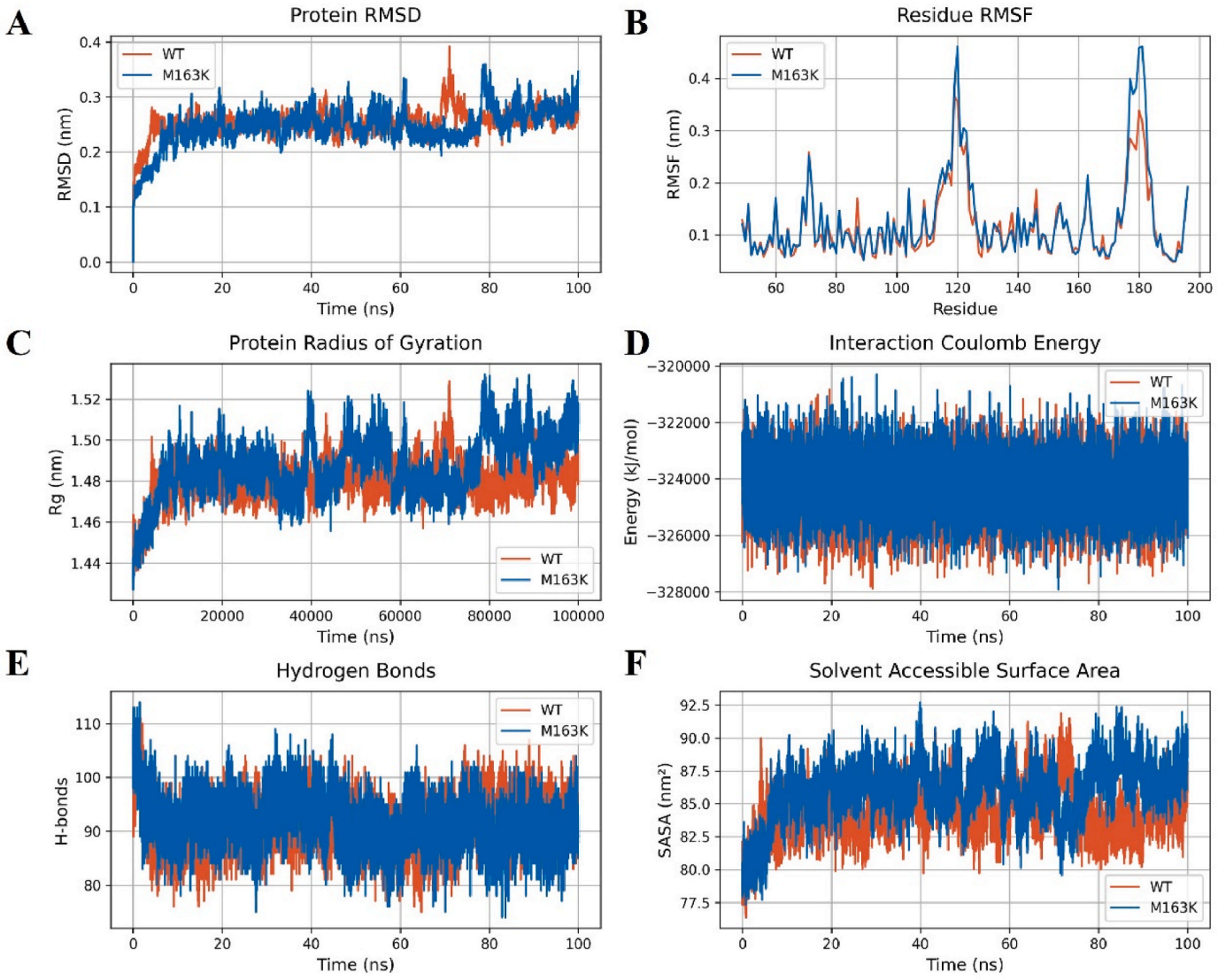


**Fig. 9.** Molecular dynamics simulation results of WT and M163K mutant. (A) Protein RMSD of the WT and M163K mutant over 100 ns of simulation. (B) Residue RMSF of the WT and M163K mutant over 100 ns. (C) Protein Rg of the WT and M163K mutant, indicating the compactness of the protein. (D) Interaction Energy of the WT and M163K mutant. (E) Hydrogen Bonds observed during the simulation. (F) SASA of the WT and M163K mutant, indicating the surface area of the protein exposed to solvent.

electrostatic contacts or hydrogen bonds. Previous studies have shown that optimization of charge–charge interactions can improve protein stability (Strickler et al., 2006), and computationally guided salt-bridge design has also been demonstrated to enhance protein thermostability (Lee et al., 2014). Therefore, the improved thermostability of M163K may be associated with strengthened intramolecular stabilizing interactions, reduced local flexibility, and enhanced resistance to thermal perturbation.

Overall, the MD results suggest that the M163K mutation may enhance the structural stability of SOD without markedly altering its interaction with $AFB_1$. Replacing methionine with lysine may reorganize the local interaction network around residue 163, favoring additional stabilizing contacts and a tighter overall fold, which could account for the enhanced thermal resistance of M163K.

## 4. Conclusion

In summary, an $AFB_1$-degrading strain, HNGD-122, was newly isolated from peanut-field soil, and an SOD with $AFB_1$-degrading activity was identified and functionally validated from this strain. PROSS-assisted protein engineering was subsequently applied to generate the M163K variant, which largely retained its $AFB_1$-degrading activity while exhibiting markedly improved thermostability, storage stability, and freeze-drying tolerance. Molecular dynamics simulations suggested that the enhanced stability of M163K may be associated with strengthened local stabilizing interactions and reduced structural flexibility. Furthermore, M163K effectively reduced $AFB_1$ residues in naturally contaminated corn flour and corn bran. Collectively, the newly isolated *Priestia megaterium*-related strain HNGD-122 and its $AFB_1$-degrading SOD further enrich the microbial and enzymatic resources available for $AFB_1$ biodetoxification. Meanwhile, the successful engineering of M163K demonstrates the feasibility of PROSS-assisted stability engineering for improving the stability and practical performance of such enzymes, providing experimental support for the development of more robust biocatalysts for $AFB_1$ mitigation.

## CRediT authorship contribution statement

**Yan Zhang:** Writing – original draft, Software, Methodology, Formal analysis, Data curation. **Yiqian Zhang:** Writing – review & editing,

Methodology. **Fred Mwabulili:** Writing – review & editing, Methodology. **Yuhui Yang:** Methodology. **Yanli Xie:** Writing – review & editing, Visualization, Supervision, Methodology, Funding acquisition, Conceptualization. **Antonio Francesco Logrieco:** Methodology.

## Ethics declaration

This study was conducted in accordance with the ARRIVE (Animal Research: Reporting of In Vivo Experiments) guidelines. This study was approved by the Animal Ethics Committee of Zhengzhou University. (Approval No. ZZUIRB2022-92)

## Ethical statements

This experiment refers to "CCAC guidelines: Zebrafish and other small, warm-water laboratory fish" and "Guidelines for Use of Zebrafish in Research, Teaching, and Testing", and strictly adheres to their ethical requirements for zebrafish laboratory animals. This experiment was approved by the Institutional Animal Care and Use Committee of Zhengzhou University (Permit Number: ZZUI RB 2022-92).

## Declaration of competing interest

√The authors declare that they have no known competing financial interests or personal relationships that could have appeared to influence the work reported in this paper.

## Acknowledgments

This work was supported by the Key Joint Funds of the National Natural Science Foundation of China (No. U24A20473), the Key R&D Projects in Henan Province (No. 231111113300), and the Cultivation Project of Tuoxin Team in Henan University of Technology (No. 2024TXTD08).

## Appendix A. Supplementary data

Supplementary data to this article can be found online at https://doi.org/10.1016/j.fbio.2026.109983.

## Data availability

Data will be made available on request.

## References

Adebo, O., Njobeh, P., Gbashi, S., Nwinyi, O., & Mavumengwana, V. (2017). Review on microbial degradation of aflatoxins. *Critical Reviews in Food Science and Nutrition, 57*(15), 3208–3217.

Arsenide, G., Phosphide, I., & Pentoxide, V. (2006). *IARC monographs on the evaluation of carcinogenic risks to humans*. Lyon, France: IARC.

Arsiccio, A., Giorsello, P., Marenco, L., & Pisano, R. (2020). Considerations on protein stability during freezing and its impact on the freeze-drying cycle: A design space approach. *Journal of Pharmaceutical Sciences, 109*(1), 464–475.

Battilani, P., Toscano, P., Van der Fels-Klerx, H., Moretti, A., Camardo Leggieri, M., Brera, C., Rortais, A., Goumperis, T., & Robinson, T. (2016). Aflatoxin $B_1$ contamination in maize in Europe increases due to climate change. *Scientific Reports, 6*(1), Article 24328.

Benkerroum, N. (2020). Chronic and acute toxicities of aflatoxins: Mechanisms of action. *International Journal of Environmental Research and Public Health, 17*(2), 423.

Bhatnagar, B. S., Bogner, R. H., & Pikal, M. J. (2007). Protein stability during freezing: Separation of stresses and mechanisms of protein stabilization. *Pharmaceutical Development and Technology, 12*(5), 505–523.

Cheng, S., Wu, T., Zhang, H., Sun, Z., Mwabulili, F., Xie, Y., Sun, S., Ma, W., Li, Q., & Yang, Y. (2023). Mining lactonase gene from aflatoxin $B_1$-degrading strain Bacillus megaterium and degrading properties of the recombinant enzyme. *Journal of Agricultural and Food Chemistry, 71*(51), 20762–20771.

Escrivá, L., Agahi, F., Vila-Donat, P., Mañes, J., Meca, G., & Manyes, L. (2021). Bioaccessibility study of aflatoxin $B_1$ and ochratoxin A in bread enriched with fermented milk whey and/or pumpkin. *Toxins, 14*(1), 6.

Eskola, M., Kos, G., Elliott, C. T., Hajšlová, J., Mayar, S., & Krska, R. (2020). Worldwide contamination of food-crops with mycotoxins: Validity of the widely cited 'FAO estimate'of 25%. *Critical Reviews in Food Science and Nutrition, 60*(16), 2773–2789.

Goldenzweig, A., Goldsmith, M., Hill, S. E., Gertman, O., Laurino, P., Ashani, Y., Dym, O., Unger, T., Albeck, S., & Prilusky, J. (2016). Automated structure-and sequence-based design of proteins for high bacterial expression and stability. *Molecular Cell, 63*(2), 337–346.

Goris, M., Cea-Rama, I., Puntervoll, P., Ree, R., Almendral, D., Sanz-Aparicio, J., Ferrer, M., & Bjerga, G. E. K. (2023). Increased thermostability of an engineered flavin-containing monooxygenase to remediate trimethylamine in fish protein hydrolysates. *Applied and Environmental Microbiology, 89*(6). e00390-00323.

Guan, Y., Chen, J., Nepovimova, E., Long, M., Wu, W., & Kuca, K. (2021). Aflatoxin detoxification using microorganisms and enzymes. *Toxins, 13*(1), 46.

Hollingsworth, S. A., & Dror, R. O. (2018). Molecular dynamics simulation for all. *Neuron, 99*(6), 1129–1143.

Hou, M., Muzaffar, N., Xie, Y., Huang, Q., Yang, Y., & Chang, G. (2026). Mechanism and application of thermostable superoxide dismutase from Alcaligenes faecalis HNGD-HTN06 to degrade $AFB_1$/ZEN. *Journal of Agricultural and Food Chemistry, 74*(3), 3081–3100.

Iqbal, S. Z., Jinap, S., Pirouz, A., & Faizal, A. A. (2015). Aflatoxin M1 in milk and dairy products, occurrence and recent challenges: A review. *Trends in Food Science & Technology, 46*(1), 110–119.

Karunnanithy, V., Abdul Rahman, N. H. B., Abdullah, N. A. H., Fauzi, M. B., Lokanathan, Y., Min Hwei, A. N., & Maarof, M. (2024). Effectiveness of lyoprotectants in protein stabilization during lyophilization. *Pharmaceutics, 16*(10), 1346.

Kumar, V., Bahuguna, A., Ramalingam, S., Dhakal, G., Shim, J.-J., & Kim, M. (2022). Recent technological advances in mechanism, toxicity, and food perspectives of enzyme-mediated aflatoxin degradation. *Critical Reviews in Food Science and Nutrition, 62*(20), 5395–5412.

Lee, C.-W., Wang, H.-J., Hwang, J.-K., & Tseng, C.-P. (2014). Protein thermal stability enhancement by designing salt bridges: A combined computational and experimental study. *PLoS One, 9*(11), Article e112751.

Loi, M., De Leonardis, S., Ciasca, B., Paciolla, C., Mulè, G., & Haidukowski, M. (2023). Aflatoxin $B_1$ degradation by Ery4 laccase: From in vitro to contaminated corn. *Toxins, 15*(5), 310.

Lyagin, I., & Efremenko, E. (2019). Enzymes for detoxification of various mycotoxins: Origins and mechanisms of catalytic action. *Molecules, 24*(13), 2362.

Ma, R., Muzaffar, N., Xu, W., Jia, H., Liang, Y., Chang, G., Yang, Y., & Xie, Y. (2025). Functional characterization and mechanism of two Aflatoxin $B_1$-Degrading enzymes from Pseudomonas aeruginosa HNGD-JZ06. *Journal of Agricultural and Food Chemistry, 73*(46), 29886–29899.

Mahato, D. K., Lee, K. E., Kamle, M., Devi, S., Dewangan, K. N., Kumar, P., & Kang, S. G. (2019). Aflatoxins in food and feed: An overview on prevalence, detection and control strategies. *Frontiers in Microbiology, 10*, 2266.

Min, L., Fink-Gremmels, J., Li, D., Tong, X., Tang, J., Nan, X., Yu, Z., Chen, W., & Wang, G. (2021). An overview of aflatoxin $B_1$ biotransformation and aflatoxin M1 secretion in lactating dairy cows. *Animal Nutrition, 7*(1), 42–48.

Moretti, A., Pascale, M., & Logrieco, A. F. (2019). Mycotoxin risks under a climate change scenario in Europe. *Trends in Food Science & Technology, 84*, 38–40.

Muzaffar, N., Ma, W., Yang, Y., Li, Q., Jia, H., & Xie, Y. (2025). Bacillus amyloliquefaciens HNGD-DF2 from Chinese Tofu: A potential thermophilic agent for $AFB_1$ and ZEN degradation in wheat and maize. *Food Control, 172*, Article 111178.

Mwabulili, F., Li, P., Li, Q., Sun, S., Yang, Y., Ma, W., Li, X., Jia, H., & Xie, Y. (2026). Effective degradation of aflatoxin $B_1$ and zearalenone by a recombinant laccase from Heyndrickxia shackletonii. *World Journal of Microbiology and Biotechnology, 42*(4), 194.

Perry, J., Shin, D., Getzoff, E., & Tainer, J. (2010). The structural biochemistry of the superoxide dismutases. *Biochimica et Biophysica Acta (BBA)-Proteins and Proteomics, 1804*(2), 245–262.

Pożarska, A., Karpiesiuk, K., Kozera, W., Czarnik, U., Dąbrowski, M., & Zielonka, Ł. (2024). $AFB_1$ toxicity in human food and animal feed consumption: A review of experimental treatments and preventive measures. *International Journal of Molecular Sciences, 25*(10), 5305.

Qin, X., Xin, Y., Zou, J., Su, X., Wang, X., Wang, Y., Zhang, J., Tu, T., Yao, B., & Luo, H. (2021). Efficient degradation of aflatoxin $B_1$ and zearalenone by laccase-like multicopper oxidase from Streptomyces thermocarboxydus in the presence of mediators. *Toxins, 13*(11), 754.

Rennison, A., Winther, J. R., & Varrone, C. (2021). Rational protein engineering to increase the activity and stability of is PETase using the PROSS algorithm. *Polymers, 13*(22), 3884.

Rushing, B. R., & Selim, M. I. (2019). Aflatoxin $B_1$: A review on metabolism, toxicity, occurrence in food, occupational exposure, and detoxification methods. *Food and Chemical Toxicology, 124*, 81–100.

Shu, X., Wang, Y., Zhou, Q., Li, M., Hu, H., Ma, Y., Chen, X., Ni, J., Zhao, W., & Huang, S. (2018). Biological degradation of aflatoxin $B_1$ by cell-free extracts of Bacillus velezensis DY3108 with broad pH stability and excellent thermostability. *Toxins, 10*(8), 330.

Strickler, S. S., Gribenko, A. V., Gribenko, A. V., Keiffer, T. R., Tomlinson, J., Reihle, T., Loladze, V. V., & Makhatadze, G. I. (2006). Protein stability and surface electrostatics: A charged relationship. *Biochemistry, 45*(9), 2761–2766.

Sun, H., He, Z., Xiong, D., & Long, M. (2023). Mechanisms by which microbial enzymes degrade four mycotoxins and application in animal production: A review. *Animal Nutrition, 15*, 256–274.

Verheecke, C., Liboz, T., & Mathieu, F. (2016). Microbial degradation of aflatoxin $B_1$: Current status and future advances. *International Journal of Food Microbiology, 237*, 1–9.

Wang, L.-T., Lee, F.-L., Tai, C.-J., & Kasai, H. (2007). Comparison of gyrB gene sequences, 16S rRNA gene sequences and DNA–DNA hybridization in the Bacillus subtilis group. *International Journal of Systematic and Evolutionary Microbiology, 57*(8), 1846–1850.

Wang, X., Bai, Y., Huang, H., Tu, T., Wang, Y., Wang, Y., Luo, H., Yao, B., & Su, X. (2019). Degradation of aflatoxin $B_1$ and zearalenone by bacterial and fungal laccases in presence of structurally defined chemicals and complex natural mediators. *Toxins, 11*(10), 609.

Weinstein, J. J., Goldenzweig, A., Hoch, S., & Fleishman, S. J. (2021). Pross 2: A new server for the design of stable and highly expressed protein variants. *Bioinformatics, 37*(1), 123–125.

Xiong, D., Wen, J., Lu, G., Li, T., & Long, M. (2022). Isolation, purification, and characterization of a laccase-degrading aflatoxin $B_1$ from Bacillus amyloliquefaciens B10. *Toxins, 14*, 250.

Xu, Y., Dong, H., Liu, C., Lou, H., & Zhao, R. (2023). Efficient Aflatoxin $B_1$ degradation by a novel isolate, Pseudomonas aeruginosa M-4. *Food Control, 149*, Article 109679.

Yao, Y., Shu, X., Wang, D., Kan, W., Su, P., Hu, H., Chen, X., Wang, D., Huang, S., & Wu, L. (2021). Non-enzymatic transformation of aflatoxin $B_1$ by Pseudomonas geniculata m29. *Frontiers in Microbiology, 12*, Article 724103.

Zhang, H., Zhang, S., Logrieco, A. F., Mule, G., Yang, Y., Liang, Y., Jia, H., & Xie, Y. (2026). Engineering laccase from Aspergillus terreus HNGD-TM15 with enhanced catalytic activity and thermostability for the degradation of Aflatoxin $B_1$ and zearalenone. *Journal of Agricultural and Food Chemistry*.